Single Magnetic Push-Pull Forward Converter Featuring Built-in Input Filter and Coupled-Inductor Current Doubler for 48V VRM

Peng Xu, Mao Ye and Fred C. Lee

Center for Power Electronics Systems
The Bradley Department of Electrical and Computer Engineering
Virginia Polytechnic Institute and State University
Blacksburg, VA 24061

***Abstract*- This paper proposes an improved push-pull forward converter with a single EI or EE core for all the magnetic components including the input inductor, the step-down transformer and the output inductors. This topology is essentially the modified push-pull converter with the built-in input filter and the coupled-inductor current doubler rectifier. The proposed integrated magnetics features minimized leakage inductance and an air gap in only the center leg; its winding and core losses are both lower than those of conventional integrated magnetic structures.**

I. INTRODUCTION

For high-end servers with multiple microprocessors, the distribution power architecture is adopted, where paralleled front-end converters provide a single DC distribution bus that feeds VRMs and other DC/DC converters. Each microprocessor has its own VRM in close proximity, providing an extremely high current. The voltage of such distribution bus is often +48V.

For such large step-down power conversions as from 48 V to 1.2 V, topologies with step-down transformers are generally used. Push-pull, symmetrical half-bridge, and full-bridge converters are the suitable topologies for this application [1]. An improved topology - push-pull forward converter has been proposed recently; it has improved transient response and increased efficiency [2].

This paper proposes an improved push-pull forward converter with a single EI or EE core for all the magnetic components including the input inductor, the step-down transformer and the output inductors. The transformer's primary and secondary windings, as well as the inductor windings, are wound on the two outer legs. Only the center leg has an air gap. The flux ripple is cancelled in the center leg, resulting in a lower core loss in the center leg.

The proposed topology is essentially the modified push-pull converter with the built-in input filter and the coupled-inductor current-doubler rectifier. Due to coupled output inductors, inductor current ripples are greatly reduced, thus increasing efficiency. This topology also provides a smooth input current with a built-in input filter. The built-in input filter is formed by the leakage inductance between the transformer's primary windings and the clamping capacitors.

Section II introduces push-pull forward converter with the current-doubler rectifier; Section III reviews existing integrated magnetic structures for the current-doubler rectifier; Section IV presents the improved integrated magnetics for the current-doubler rectifier; Section V proposes the single magnetic push-pull forward converter and its designs and experimental results for 48-V VRM.

II. PUSH-PULL FORWARD CONVERTER WITH CURRENT DOUBLER RECTIFIER

Fig. 1 shows the push-pull forward converter. It has an improved transient response and increased efficiency. This topology is essentially a modified push-pull converter topology with a clamp capacitor.

For low-voltage, high-current applications, the secondary-side power losses have a major impact on the conversion efficiency. The secondary-side losses can be reduced by using the current-doubler topology, due to its simpler transformer secondary winding and two times lower inductor currents and transformer secondary currents [3,4,5,6,7].

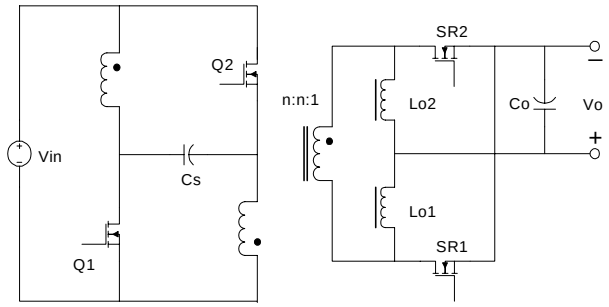

Fig. 1. Push-pull forward converter with the current-doubler rectifier.

Besides the efficiency, the transient response is another major concern for VRMs. The transient response can be improved by reducing the output filter inductance so that the slew rate of the inductor current is maximized during the transients. Due to the ripple cancellation in the current-doubler rectifier, the large ripple currents generated by small inductors are canceled at VRM output.

In summary, the push-pull forward converter with the current doubler rectifier is a suitable topology for 48-V VRM applications.

This work was supported by Delta Electronics, Hipro, Hitachi, IBM, Intel, Intersil, National Semiconductors, Power-One, TDK and Texas Instruments.

This work made use of ERC Shared Facilities supported by the National Science Foundation under Award Number EEC-9731677.

III. Existing Integrated Magnetics for Current-Doubler

A. Review of Existing Integrated Magneitcs

The transformer and the filter inductors in the current-doubler rectifier can be integrated into a single magnetic EE or EI core. Fig. 2 shows the discrete magnetic implementation and several existing integrated magnetic implementations for the current doubler rectifier.

Fig. 2(a) shows the discrete magnetic implementation for the current-doubler rectifier. Three magnetic cores, three high-current windings and five high-current interconnections are needed.

Fig. 2(b) shows the integrated magnetics structure proposed by O. Seiersen [4]. A single conventional EE or EI core is used with air gaps in the outer legs only. The implementation reduces the overall size of the magnetics, since the transformer and two inductors share the outer legs of the core. Three high-current windings and five high-current interconnections are still needed.

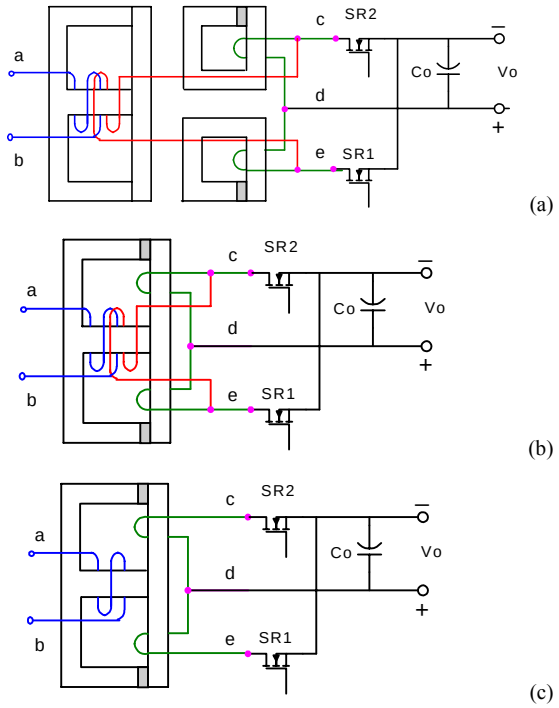

Fig. 2. Implementations of current doubler: (a) discrete magnetic, (b) Seiersen's integrated magnetics, and (c) fully integrated magnetics.

Fig. 2(c) shows an improved integrated magnetics structure [8]. Both core and winding integration are realized in this structure. Not only do the transformer and two inductors share the the core, but the transformer secondary winding and inductor windings are also integrated together. Only two high-current windings and three high-current interconnections are needed. For high-current applications, this winding integration becomes more important because of its lower interconnection loss and lower conduction loss. As a result, this integrated magnetic structure allows for lower overall system cost and size, as well as higher efficiency.

B. Limitations of Existing Integrated Magneitcs

Despite all the advantages described in the preceding section, the existing integrated magnetic structure also has some drawbacks.

Fig. 3 illustrates the core structure of the integrated magnetics, with only one winding shown for simplification. The air gaps are placed on the two outer legs and there is no air gap in the center leg in order to avoid the interaction between the two flux loops.This kind of magnetic core is not a standard industry practice; the precise gapping adjustment and filling are requested, which means mass production difficult and costly. Besides the cost, the two pieces of the core are connected only at the center leg, rendering the structure mechanically unstable. Moreover, the existence of air gaps on the two outer legs also causes an electromagnetic interference (EMI) issue.

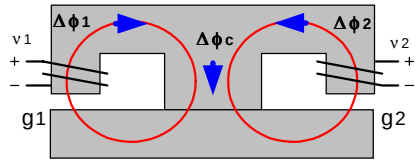

Fig. 3. Core structure of existing integrated magnetics.

Another drawback is that the transformer in the existing integrated magnetics has a large leakage inductance. As shown in Fig. 4, the transformer's primary windings are wound around the center leg while the transformer's secondary windings are wound on the two outer legs. A significant leakage flux exists in the transformer windings, and the coupling between the transformer's primary and secondary windings is poor. Consequently, the transformer in the integrated magnetics has a large leakage inductance, causing severe parasitic ringing across switching devices, decreasing the effective duty cycle at the secondary, and impairing efficiency.

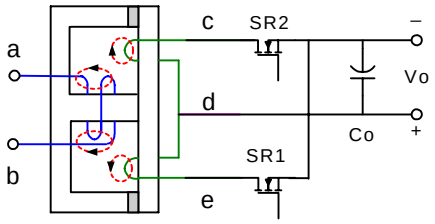

Fig. 4. Large leakage flux in existing integrated magnetics.

IV. Proposed Integrated Magnetics for Current-Doubler

In order to improve both the core structure and the transformer performance of existing integrated magnetics, a novel magnetic integration approach is proposed as follows.

A. Derivation of Improved Integrated Magnetics

Fig. 5 shows the approach for deriving the improved integrated magnetic structure with minimized leakage inductance and an air gap in only the center leg. The discussion begins with the existing integrated magnetics structure shown in Fig. 2(c).

Step 1: The transformer's primary winding is split between two outer legs, as shown in Fig. 5(a), without changing the flux distributions. Since both the primary and secondary windings are wound on the two outer legs, interleaving can be used to minimize the leakage inductance of the integrated transformer.

Step 2: The polarity of one set of windings is changed through different winding connections, as shown in Figure 5(b). Correspondingly, the direction of flux is changed as well. Before the change, the DC flux circulates between the two outer legs and no DC flux exists in the center leg. The air gaps on the outer legs prevent saturation of the core. After the change, no DC flux circulates between the two outer legs.

Step 3: As shown in Fig. 5(b), since there is no DC flux circulating between the two outer legs, the air gaps in the outer legs can be shifted to the center leg while keeping the core unsaturated, as shown in Fig. 5(c).

Fig. 5(c) shows the proposed integrated magnetic structure, in which the transformer's primary and secondary windings are wound on the two outer legs. Thus, the integrated transformer offers minimized leakage inductance. Moreover, the core structure has an air gap in the center leg and no air gap in the outer legs; this is the standard industry practice and is much easier to manufacture.

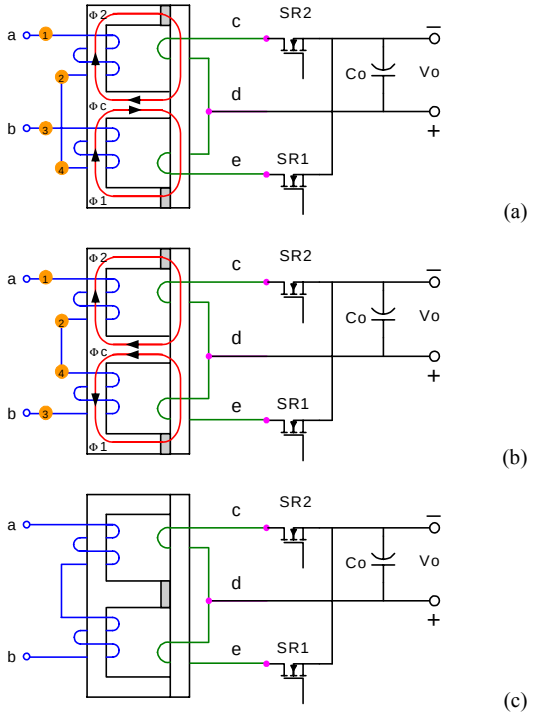

Fig. 5. A novel integrated magnetic structure for the current-doubler rectifier.

B. Analysis of Proposed Integrated Magnetic Circuit

Fig. 6 shows the reluctance model for the proposed magnetic circuit. The windings are represented as the magnetomotive force (MMF) sources. The R_O and R_C represent the reluctances of the outer and center legs, respectively. The current directions are defined according to device conduction states. The major flux directions are determined by using Right-Hand Rule.

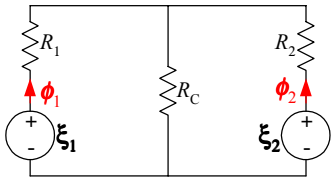

Fig. 6. Magnetic reluctance circuit of proposed integrated magnetics.

The electrical circuit model can be derived from the magnetic model using the principle of duality. The equivalent electrical circuit is the current-doubler rectifier, where two output inductors are reverse-coupled [10], as shown in Fig. 7.

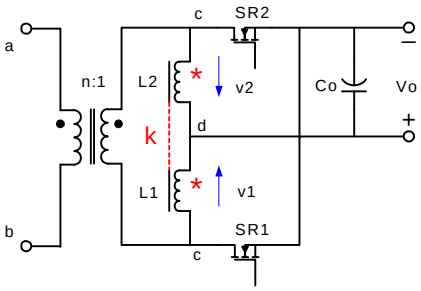

Fig. 7. Equivalent electrical circuit of proposed integrated magnetics circuit.

Assuming L1=L2=L, and that the mutual inductance between L1 and L2 is M, and the coupling coefficient is k, the analytical relationship between inductances and reluctances can be derived as follows:

$$L = \frac{Ns^2 \cdot (Ro + Rc)}{Ro \cdot (Ro + 2 \cdot Rc)}$$
$$M = \frac{Ns^2 \cdot Rc}{Ro \cdot (Ro + 2 \cdot Rc)} \quad (1)$$
$$k = \frac{M}{L} = \frac{Rc}{Ro + Rc}$$

In the proposed integrated magnetics, only the center leg has an air gap. The reluctance in the center leg is much larger than those of the outer legs. Equation 1 can be simplified as follows:

$$L \approx \frac{Ns^2}{2 \cdot Ro}$$
$$M \approx \frac{Ns^2}{2 \cdot Ro} \quad (2)$$
$$k = \frac{M}{L} \approx 1$$

As can be seen from Equation 2, without considering the reluctance from the magnetic material, the coupling coefficient for the two inductors is close to one. However, "Close to one" does not mean "equal to one". The increase in the coupling coefficient is achieved by the increase in both the self- and mutual inductances. Two coupled inductors still have a certain amount of leakage inductance.

In practice, the reluctances from the magnetic material influence the value of Ro and Rc, and the typical coupling coefficient k is in the range of 0.8 to 0.9.

C. *Flux Distributions*

Fig. 8 shows the AC fluxes in the proposed integrated magnetics. According to Farad's Law, the AC fluxes in the two outer legs, $\Delta\phi 1$ and $\Delta\phi 2$, are the time integral of the voltages across corresponding windings. For both the existing and the proposed structure, the winding voltage waveforms are the same. The magnitude of the AC fluxes in the two outer legs can be derived as follows:

$$\Delta\varphi 1 = \Delta\varphi 2 = \frac{Vo \cdot (1 - D)}{Ns \cdot Fs} \tag{3}$$

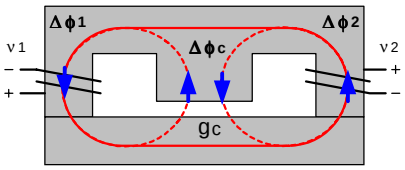

Fig. 8. AC fluxes in the core of proposed integrated magnetics.

The AC flux in the center leg is the sum of the AC fluxes in the two outer legs. In the existing structure, the AC fluxes are added in the center leg, as shown in Fig. 3. The magnitude of AC flux in the center leg can be derived as follows:

$$\Delta\varphi c = \frac{Vo}{Ns \cdot Fs} \tag{4}$$

In the proposed structure, the polarity of one set of windings is changed; therefore, the direction of AC flux in one of the two outer legs is also changed. Consequently, the AC fluxes are canceled in the center leg. The magnitude of AC flux in the center leg can be derived as follows:

$$\Delta\varphi c' = \frac{Vo \cdot (1 - 2D)}{Ns \cdot Fs} \tag{5}$$

With the reduction of the magnitude of AC flux in the center leg, the proposed integrated magnetics has a lower core loss in the center leg. Fig. 9 shows the FEA results of the AC flux distribution in the core of the proposed integrated magnetics.

Another advantage of the AC flux cancellation in the center leg is the much smaller fringing effects and fewer EMI problems caused by the air gap. Large air gaps are usually associated with fringing effects and EMI problems. However, in the proposed structure, the AC flux through the air gap in the center leg is much smaller. The fringing effects associated with the center leg air gap are much smaller. The Less eddy currents generated in the windings, the lower winding loss.

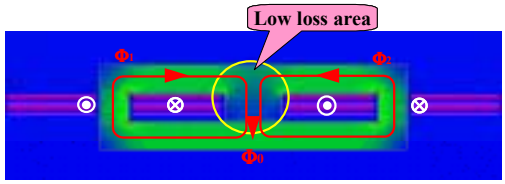

Fig. 9. AC flux cancels in the center leg of the core in proposed structure.

Another important factor in integrated magnetic design is the DC flux bias in the core. Fig. 10 shows the DC flux bias in the cores of both existing and proposed structures.

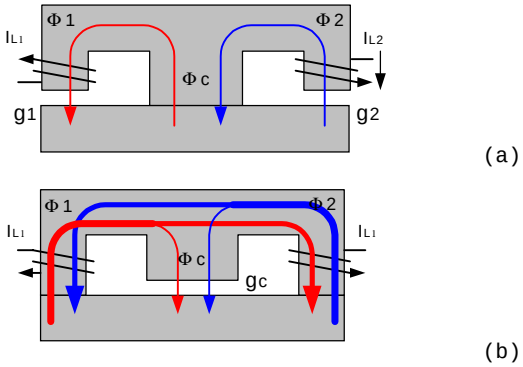

Fig. 10. DC flux bias in the core of: (a) existing structure (M=0), and (b) proposed structure.

In the existing structure, the DC fluxes generated by the two sets of windings do not affect each other. Assuming that the DC currents in the two inductors are the same (I_L=I_{L1}=I_{L2}), the DC flux in the center leg is zero. The DC flux bias in the existing structure can be derived as:

$$\Phi 1 = \Phi 2 = \frac{Ns \cdot I_L}{Ro} = \frac{L \cdot I_L}{Ns} \tag{6}$$

$$\Phi c = 0$$

For the proposed structure, the majority of the DC flux generated by one set of windings goes through the other set. Because of the inverse direction, the majority of DC flux in the two outer legs is cancelled. The percentage of the DC flux that is cancelled is proportional to the mutual inductance. Although a larger self-inductance in the proposed structure generates larger DC flux, the percentage of the cancelled DC flux is also increased. The net DC fluxes in the outer legs go through the center leg. The DC flux in the center leg is the sum of the DC fluxes in the two outer legs. The DC flux bias in the existing structure can be derived as:

$$\Phi 1 = \Phi 2 = \frac{Ns \cdot I_L}{2 \cdot Rc} = \frac{(L - M) \cdot I_L}{Ns} \tag{7}$$

$$\Phi c = \frac{Ns \cdot I_L}{Rc} = \frac{2 \cdot (L - M) \cdot I_L}{Ns}$$

According to Equations 6 and 7, with the same value for L-M (M=0 in the existing structure), the existing and proposed integrated magnetic structures have equal DC flux biases in the two outer legs. Assuming that the cross-section area of the center leg is twice that of each the outer leg, the same length of air gap for both structures achieves equal DC fluxes in the two outer legs.

D. Inductor Coupling Effect

As shown in Fig. 7, the two inductors are inversely coupled. In order to see the effect of inductor coupling, the concept of equivalent inductance is adopted, which is proposed by P. Wong and is used to analyze the coupled inductors in two-phase buck converter [9].

Fig. 11 shows the inductor voltage and current waveforms during the transient for the non-coupling and coupling cases. The steady-state inductor current waveform is the solid line, while the transient inductor current waveform is the dotted line. Assuming the duty cycle has an increase of ΔD during the transient, the inductor current has an increase of Δi after a switching cycle.

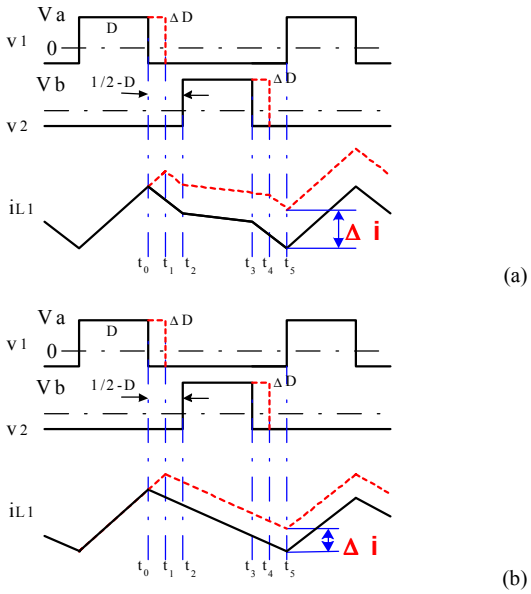

Fig. 11. Inductor voltage and current waveforms during the transient: (a) the coupling case, and (b) the non-coupling case.

For the non-coupling case, Δi can be derived as follows:

$$\Delta i_{NC} = \frac{(Vs + Vb)\cdot \Delta D}{L \cdot Fs} \tag{8}$$

For the coupling case, Δi can be derived as follows:

$$\Delta i_{CP} = \frac{(Va + Vb)\cdot \Delta D}{(L - M)\cdot Fs} \tag{9}$$

Comparing Equations 8 and 9, with the same value for L-M (M=0 in the existing structure), the two magnetic circuits have the same transient inductor slew rates.

Fig. 12 shows the steady-state inductor voltage and current waveforms for the non-coupling and coupling cases. The solid lines corresponds to the coupling case, while the dashed lines corresponds to the non-coupling case.

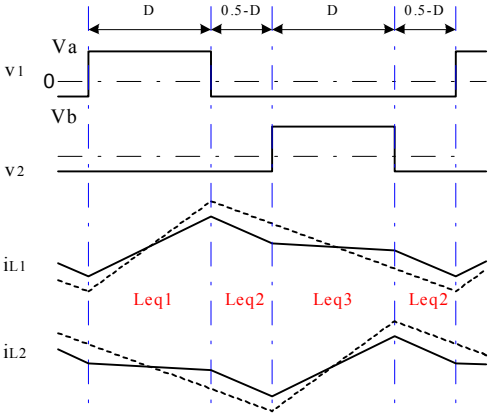

Fig. 12. Steady-state voltage and current waveforms for the coupling and non-coupling cases.

The steady-state inductor peak-to-peak current for the non-coupling case is derived as follows:

$$I_{PP\_NC} = \frac{Va \cdot D}{L \cdot Fs} \tag{10}$$

The steady-state inductor peak-to-peak current for the coupling case is derived as follows:

$$I_{PP\_CP} = \frac{Va \cdot D}{(L - M)\cdot Fs} \cdot \frac{L - \frac{D}{1-D}\cdot M}{L + M} \tag{11}$$

A large inductance is preferred so that the current ripples can be reduced. Comparing Equations 10 and 11, with the same transient equivalent inductance (L-M), the steady-state current ripple of the coupling case is always smaller than that of the non-coupling case.

Another important factor is the effect of coupling on the output current. The output current is the sum of the inductor currents. The output current for the coupling case can be derived as follows:

$$v_1 + v_2 = (L - M)\cdot \frac{d(i_{L1} + i_{L2})}{dt} = (L - M)\cdot \frac{di_O}{dt} \tag{12}$$

The output current for the non-coupling case can be derived as follows:

$$v_1 + v_2 = L \cdot \frac{d(i_{L1} + i_{L2})}{dt} = L \cdot \frac{di_O}{dt} \tag{13}$$

Comparing Equations 12 and 13, with the same transient equivalent inductance (L-M), the output current waveforms are the same for both the coupling and non-coupling cases.

In summary, with the same transient equivalent inductance (L-M), the steady-state current ripple of the coupling case is always smaller than that of the non-coupling case, while the output current waveforms are the same for both cases.

V. Single Magnetic Push-Pull Forward Converter

A. Concept of Built-in Input Filter

The preceding magnetic integration approach only combines the transformer with output filter inductors. The issue of further integration of the input filter inductor is addressed in this section. With the proposed structure, it is possible to use only a single magnetic core for entire converters.

Fig.13 shows the push-pull forward converter with the proposed integrated magnetics for the current doubler rectifier. Fig. 14 shows its electrical equivalent circuits.

Two circuits shown in Fig. 14 are exchangeable. The circuit shown in Fig. 14(b) is used for the following discussion, since the split transformer windings are shown in this circuit, which corresponds to the physical implementations shown in Fig. 13.

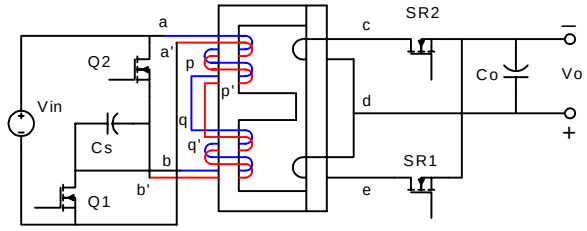

Fig. 13. Push-pull forward converter with proposed integrated magnetics.

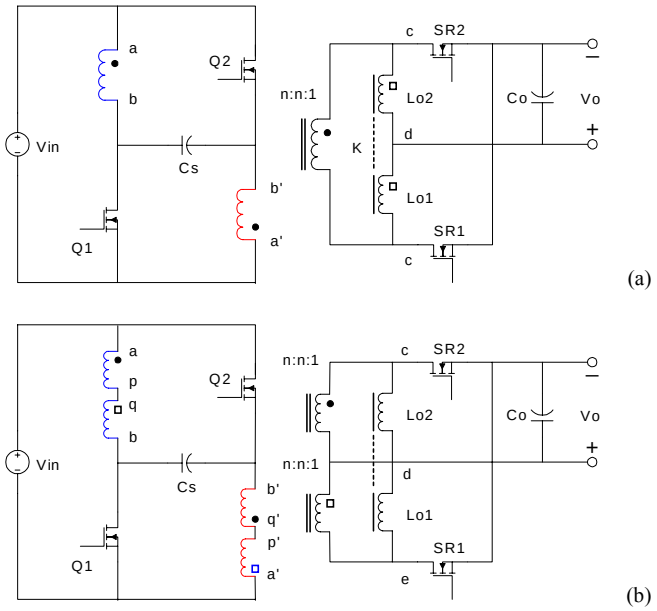

Fig. 14. Electrical equivalent circuits of push-pull forward converter with proposed integrated magnetics: (a) without showing split transformer windings, and (b) with showing split transformer windings.

An improved push-pull forward converter is proposed, as shown in Fig. 15, by splitting the clamping capacitor Cs into two pieces and meanwhile, changing the connections of the split primary windings and the primary switching devices.

The improved push-pull forward converter features a built-in input filter. The operation waveforms for both converters are the same except the input current. In the improved push-pull forward converter, the input current is near ripple free, while the original converter exhibits a pulsing input current.

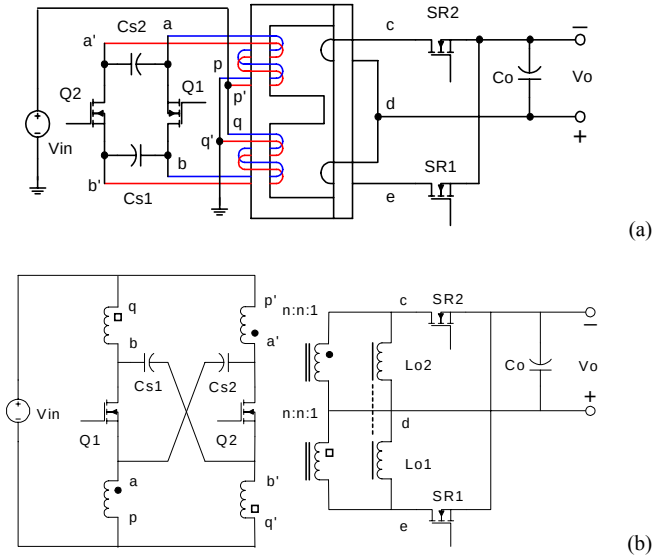

Fig. 15. Improved push-pull forward converter: (a) implementation with integrated magnetics; and (b) electrical equivalent circuit.

As shown in Fig. 13 and 15, the same integrated magnetic structure is used for both the original and improved push-pull forward converters. In the improved push-pull forward converter, the built-in input filter is formed by the leakage inductance and the clamping capacitors. The suitable leakage inductance of the transformer windings is utilized as the input filter inductor, while the clamping capacitors are serving as the filter capacitors. The concept of built-in filters has also been used for other applications [13,14,15].

Because of the existence of the built-in input filter, the input filter size can be reduced for the improved push-pull forward converter, and sometimes even no external input filter is needed. It is possible to use only a single magnetic core for entire converters.

B. 48V VRM Prototype and Experimental Results

48V-input, 1.2V/70A-output VRM prototype was built using the single magnetic push-pull forward converter. The prototypes operate at 100kHz. The following components are selected for the power stage: primary switch – PSMN035-150B (150v, 35mohm); secondary switch – 2xSTV160NF03L (30V, 3mohm); and output inductance – 320nH. Fig. 16 shows the photograph of this 48V VRM prototype.

The magnetic core is a combination of E32-3F3 and PLT32-3F3. The center leg has a 10mil air gap. The windings are embedded in 2-oz 9-layer PCB. Two primary windings

have eight turns each with four turns per layer. The secondary windings use a single turn with five layers paralleled. The leakage inductance measured at the primary side is about 1.4 uH. Two clamping capacitors are both 3.3uF.

Fig. 16. 48V VRM prototype using single magnetic push-pull forward converter.

Fig. 17 shows the experimental waveforms at full load. With the integrated input filter, the input current is smooth in the improved push-pull forward converter.

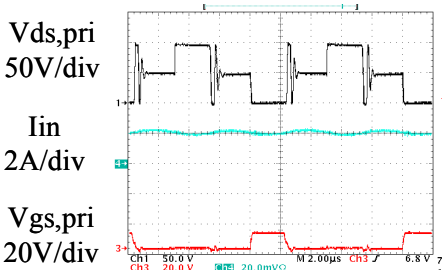

Fig. 17. Experimental waveforms at full load for single magnetic push-pull forward converter.

Fig. 18 shows the measured efficiency. The improved push-pull forward converter achieves a 91% ceiling efficiency and an 85% full-load efficiency. Compared to the conventional push-pull converter, the improved push-pull forward converter has more than 3% efficiency improvement. Compared to the original push-pull forward converter, the integration of the input filter also helps improve the efficiency, especially at light load.

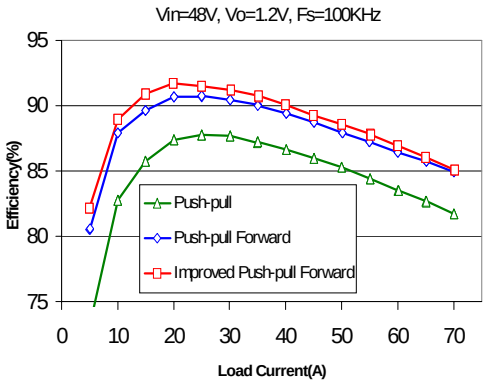

Fig. 18. Measured VRM efficiency.

VI. Conclusion

In the push-pull forward topology, an integrated magnetics structure has been proposed for the current-doubler rectifier in order to make the high-input VRM more efficient, more compact and less expensive, where the transformer's primary and secondary windings, as well as the inductor windings, are wound on the two outer legs. An improved push-pull forward converter has been proposed further by utilizing the leakage inductance of the integrated magnetics and the clamping capacitors for the input filter. With the built-in input filter, we can reduce the size and improve the efficiency further.

References

[1] Y. Panvo and M. M. Jovanovic, "Design and Performance Evaluation of Low-Voltage/High-Current DC/DC On-Board Modules," *IEEE APEC*, 1999.

[2] X. Zhou, B. Yang, L. Amoroso, F. C. Lee and P. Wong, "A Novel High-input-voltage, High Efficiency and Fast Transient Voltage Regulator Module: The Push-pull Forward Converter," *IEEE APEC*, 1999.

[3] O. Seiersen, "Power Supply Circuit," *U. S. Patent 4899271*, February 6, 1990.

[4] C. Peng, M. Hannigan, O. Seiersen, "A new efficient high frequency rectifier circuit", *HFPC*, 1991, pp. 236-243.

[5] K. O'Meara, " A New Output Rectifier Configuration Optimized for High Frequency Operation," *HFPC*, 1991, pp. 219-226.

[6] L. Balogh, "The Performance of the Current Doubler Rectifier with Synchronous Rectification," *HFPC*, 1995, pp. 216-225.

[7] L. Huber and M. Jovanovic, "Forward Converter with Current-Doubler Rectifier: Analysis, Design, and Evaluation Results," *IEEE APEC*, 1997, pp. 605-611.

[8] W. Chen, G. Hua, D. Sable, F. C. Lee, "Design of high efficiency, low profile, low voltage converter with integrated magnetics," *IEEE APEC*, 1997, pp. 911-917.

[9] P. Wong, Q. Wu, P. Xu, B. Yang and F. C. Lee, "Investigating Coupling Inductor in Interleaving QSW VRM," *IEEE APEC*, 2000, pp. 973-978.

[10] A. Pietkiewicz and D. Tollik, "Coupled-Inductor Current-Doubler Topology in Phase-Shifted Full-Bridge DC-DC Converter," *IEEE INTELEC*, 1998, pp. 41-48.

[11] P. Xu, Q. Wu, P. Wong and F. C. Lee, "A Novel Integrated Current-Doubler Rectifier," *IEEE APEC*, 2000.

[12] P. Xu and F. C. Lee, "Design of High-Input Voltage Regulator Modules With A Novel Integrated Magnetics," *CPES Annual Seminar*, 2000, pp. 112-115.

[13] E. Herbert, "Analysis of the Near Zero Input Current Ripple Condition in a Symmetrical Push-Pull Power Converter," *HFPC*, 1989.

[14] C. Leu and J. Hwang, "A Built-in Input Filter Forward Converter," *IEEE PESC*, 1994.

[15] R. Lai, K. D. T. Ngo, "Steady-State Analysis of the Symmetrical Push-Pull Power Converter Employing a Matrix Transformer," *IEEE Transaction on Power Electronics*, January 1992, pp. 44-52.